FRONTIERS OF PHYSICS

RESEARCH ARTICLE
Volume 22 / Issue 5 / 052201 / 2027

Electromagnetically-Induced transparency bridges disconnected light-harvesting networks

Jun Wang, Rui Li, Yi Li, Kai-Ya Zhang, Qing Ai†

School of Physics and Astronomy, Beijing Normal University, and Key Laboratory of Multiscale Spin Physics (Beijing Normal University), Ministry of Education, Beijing, 100875, China
Corresponding author. E-mail: †aiqing@bnu.edu.cn
Received February 19, 2026; accepted November 2, 2026

© Higher Education Press 2027

ABSTRACT

The energy-transfer efficiency of the natural photosynthesis system appears to be highly optimized during the evolution for millions of years. However, how to enhance the efficiency in artificial light-harvesting systems is still unclear. In this paper, we investigate the energy-transfer process in the photosystem I (PSI). When there is no effective coupling between the outer antenna and the reaction center, the two light-harvesting networks are disconnected and thus the energy transfer is inefficient. In order to repair these disconnected networks, we introduce a bridge with three sites between them. We find that by modulating the level structure of the 3-site bridge to be resonant, the energy transfer via the dark state will be enhanced and even outperform the original PSI. Furthermore, we demonstrate that the bridge scheme also enhances energy-transfer efficiency in artificial light-harvesting structures. Our discoveries may shed light on the designing mechanism of artificial light-harvesting systems.

Keywords photosynthesis, energy transfer, electromagnetically induced transparency, dark state

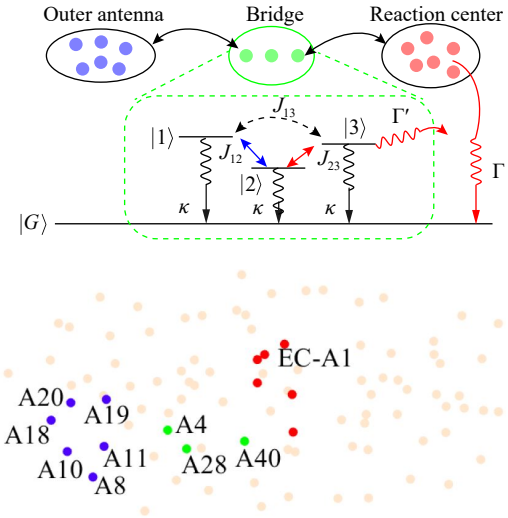

1 Introduction

The demand for sustainable energy solutions has increasingly turned to the sun, an inexhaustible source of power that holds the promise of resolving our ongoing energy crises. In natural photosynthesis, green plants and other photosynthetic organisms perform excellent efficiency of converting and storing solar energy. This biological process occurs within the chloroplasts' thylakoid membranes, whose structure has been optimized during the evolution for millions of years. Inspired by the natural photosynthesis, artificial photosynthetic systems have been fervently developed to mimic these biological processes to harness solar energy effectively [1–12].

At the heart of natural photosynthesis are photosystem I (PSI) [13] and photosystem II [14] (PSII). These multi-subunit complexes are embedded within the thylakoid membranes and are responsible for light harvesting [15]. The natural efficiency of these systems is largely due to their light-harvesting antennae, which capture a broad spectrum of wavelengths using multiple chlorophyll molecules. This large cross-sectional area of chlorophyll does not only capture sunlight efficiently but also facilitates rapid energy transfer to the reaction center (RC) [16–24]. To enhance the efficiency of artificial systems, much effort has been paid to the study of the mechanisms of PSI and PSII, aiming to replicate and optimize these processes in synthetic setups [25–36].

However, in the artificial photosynthetic systems, the outer antenna (OA) might be far away from the RC, leading to weak coupling between them. A direct solution

https://doi.org/10.15302/frontphys.2027.052201

is to insert a bridge to connect the OA and the RC. The bridge should consist of multiple sites in order to cross over a sufficiently long distance. Thus, it is crucial to optimize the bridge to reduce the dissipation of the intermediate site in the bridge. The electromagnetically-induced transparency (EIT) [37–45] offers an intriguing possibility for this problem. The EIT is a phenomenon that the population on the lossy intermediate level of a three-level system is sufficiently suppressed when the energy levels satisfy the two-photon resonance. The state without population on the intermediate level is named as the "dark state", which can be used to improve the energy transfer efficiency [46]. By applying the EIT to the energy-transfer processes in the artificial photosynthetic system, it is possible to bridge the OA and the RC in such a way that energy loss through spontaneous emission at intermediate sites is minimized, and the overall efficiency of the artificial light-harvesting system is increased.

In this paper, we investigate the energy-transfer process in an inefficient light-harvesting system including two disconnected networks. Because the OA is far away from the RC, their interaction is weak and the energy cannot be effectively transferred from the OA to the RC. In order to repair the network, we introduce a bridge with three sites between the OA and the RC. When both the single-photon and two-photon resonance conditions are satisfied, the decay via the intermediate site is suppressed during the energy-transfer process through the dark state. Furthermore, when the site energies of the three-site bridge are the same as in the natural PSI, the energy-transfer efficiency can be further optimized. However, when there is two-photon resonance but large single-photon detuning, the efficiency is slightly decreased, which implies that the natural PSI has been sufficiently optimized during the evolution in the past millions of years. Interestingly, the energy-transfer efficiency can be further optimized as compared to the natural PSI when the single-photon resonance is achieved. This bridge structure also works well in an artificial light-harvesting system. In this regard, we can repair two disconnected light-harvesting networks by introducing a bridge assisted by the EIT.

2 Model

We consider a light-harvesting system described by the density matrix ρ under the single-excitation condition. The system contains two networks, i.e., the OA and the RC, and a bridge between them, as shown in Fig. 1(a). Each site in Fig. 1(a) represents a chlorophyll modeled as a two-level system. The coherent part of the dynamics of the system can be modeled by the N-qubit Hamiltonian describing the coherent exchange of excitations between different sites, i.e.,

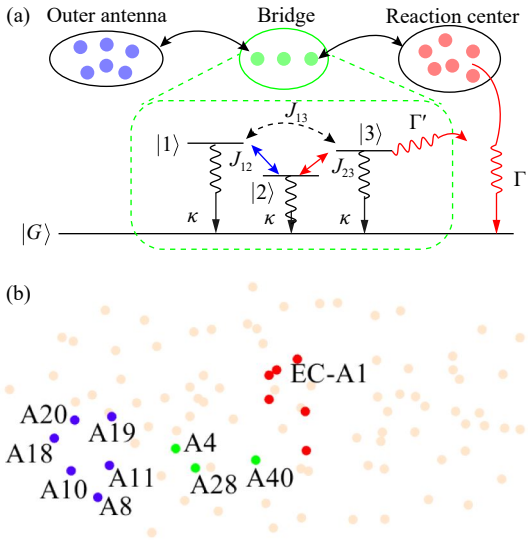

Fig. 1 **(a)** Schematic of disconnected light-harvesting networks repaired by an EIT bridge. Each dot represents a chlorophyll with a ground state and an excited state. A bridge with three sites is inserted between the OA and the RC to connect them. Under the single-excitation condition, $|m\rangle$ represents the excitation on site m, while the other sites are in the ground state. κ is the spontaneous-emission rate, and Γ represents the charge-separation rate in the RC. For the simplified 3-site bridge model, Γ' is the effective rate of site 3 in the bridge to the RC. **(b)** The position of the Mg atoms of the chlorophyll molecules in PSI. Blue, green and red dots respectively represent the OA, the bridge and the RC sites. The gray dots are the other sites in the PSI.

$$H = \sum_{n=1}^{N} E_n |n\rangle\langle n| + \sum_{m\neq n} J_{mn} |m\rangle\langle n|, \tag{1}$$

where $\hbar = 1$, $|n\rangle$ denotes a single excitation in site n, E_n is the local site energy, J_{mn} is the hopping rate of the excitation between sites m and n induced by the dipole-dipole interaction. Please refer to Ref. [47] for more details. The Hamiltonian H can be diagonalized as $H = \sum_k \varepsilon_k |\varepsilon_k\rangle\langle\varepsilon_k|$ with the eigen energy ε_k and the eigen state $|\varepsilon_k\rangle$.

We represent the biochemical reaction in the RC by the decay of the excitation on the final site labeled by $|N\rangle$ to the ground state $|G\rangle$, which is modeled by the Lindblad term $\mathcal{L}_{\rm rc}(\rho) = \Gamma\mathcal{D}(|G\rangle\langle N|)\rho$, with Γ being the biochemical-reaction rate and $\mathcal{D}(A)\rho = A\rho A^\dagger - (\rho A^\dagger A + A^\dagger A\rho)/2$. In addition, the spontaneous emission for the excitation on each site to the ground state $|G\rangle$ can be modeled by the local Lindblad term $\mathcal{L}_{\rm em}(\rho) = \sum_n \kappa\mathcal{D}(|G\rangle\langle n|)\rho$, with κ being the spontaneous-emission rate.

The coherent modified Redfield theory (CMRT) and its generalization [48–53] have been widely used to describe the energy transfer and the spectra, which yield reliable results as compared to the experiments. However, since the CMRT master equation of an M-site

system contains a set of M^2 ordinary differential equations, the simulation of the dynamics becomes demanding when the system contains hundreds of sites, e.g., 96 sites in PSI. Therefore, we utilize the non-Markovian quantum-jump method [54–61] to reduce the computational complexity. The CMRT dynamics is described by the generalized Lindblad term $\mathcal{L}_{\rm cmrt}(\rho) = \sum_{k,p} R_{kp}\mathcal{D}(|\varepsilon_k\rangle\langle\varepsilon_p|)\rho$, with R_{kp} $(k \neq p)$ being the energy-transfer rate from the eigen state $|\varepsilon_p\rangle$ to $|\varepsilon_k\rangle$ and R_{kk} being the pure-dephasing rate [57]. The detailed derivation is presented in Appendix A.

Therefore, on account of the biochemical reaction and the spontaneous emission, the master equation of the CMRT reads

$$\frac{\partial\rho}{\partial t} = -\mathrm{i}[H,\rho] + \mathcal{L}_{\rm rc}(\rho) + \mathcal{L}_{\rm em}(\rho) + \mathcal{L}_{\rm cmrt}(\rho). \tag{2}$$

The efficiency η of the light-harvesting system is [62]

$$\eta = \Gamma\int_0^\infty \langle N|\rho(t)|N\rangle \mathrm{d}t. \tag{3}$$

Here, $\Gamma\langle N|\rho(t)|N\rangle$ is the instantaneous probability flux into the irreversible charge-separation channel. Its time integral therefore gives the total probability that an initially normalized excitation undergoes charge separation rather than spontaneous-emission loss. Accordingly, η represents the charge-separation yield from initial excitation.

To investigate the effect of the dark state in the bridge, we introduce a simplified 3-site bridge model with $N = 3$ in the Hamiltonian H. The EIT effect exists under the two-photon resonance condition $E_1 = E_3$. We use $\Delta = E_1 - E_2$ to represent the single-photon detuning between the intermediate site and the other two sites. For a linear-type bridge, the large distance between the initial site 1 and the final site 3 leads to a weak coupling, i.e., $J_{13} \ll J_{12}, J_{23}$. Therefore, we set $J_{13} = 0$ for the analytical analysis. By setting E_1 as the zero-point of energy, the Hamiltonian reads $H = -\Delta|2\rangle\langle 2| + J_{12}|1\rangle\langle 2| + J_{23}|2\rangle\langle 3| + h.c.$. The eigenvalues are $\varepsilon_0 = 0$ and $\varepsilon_\pm = (-\Delta \pm \lambda)/2$, where $J^2 = J_{12}^2 + J_{23}^2$ and $\lambda = \sqrt{\Delta^2 + 4J^2}$. The eigenvalues can be simplified as $\varepsilon_+ = J\tan\phi$ and $\varepsilon_- = -J\cot\phi$ with $\tan 2\phi = 2J/\Delta$. By introducing the mixing angle $\theta = \arctan(J_{12}/J_{23})$, the eigenstates corresponding to ε_0, ε_+, and ε_- are respectively $|d\rangle = (\cos\theta, 0, -\sin\theta)^{\rm T}$, $|b_+\rangle = (\sin\theta\cos\phi, \sin\phi, \cos\theta\cos\phi)^{\rm T}$, and $|b_-\rangle = (\sin\theta\sin\phi, -\cos\phi, \cos\theta\sin\phi)^{\rm T}$, where $|d\rangle$ is the dark state and $|b_\pm\rangle$ are the two bright states.

In this framework, we begin by analytically investigating the dynamics of the bridge while neglecting dissipation. Figure 2(a) presents the population transfer from the initial state $|1\rangle$ to the target state $|3\rangle$. For $|\psi(0)\rangle = |1\rangle = \cos\theta|d\rangle + \sin\theta\cos\phi|b_+\rangle + \sin\theta\sin\phi|b_-\rangle$, the population on $|3\rangle$ at time t is $|\langle 3|\psi(t)\rangle|^2 = (\sin^2 2\theta)/4 \cdot |\cos^2\phi\exp(-\mathrm{i}\varepsilon_+ t) + \sin^2\phi\exp(-\mathrm{i}\varepsilon_- t) - 1|^2$. The fastest transfer occurs at zero single-photon detuning, i.e., $\Delta = 0$. The excitation transfer

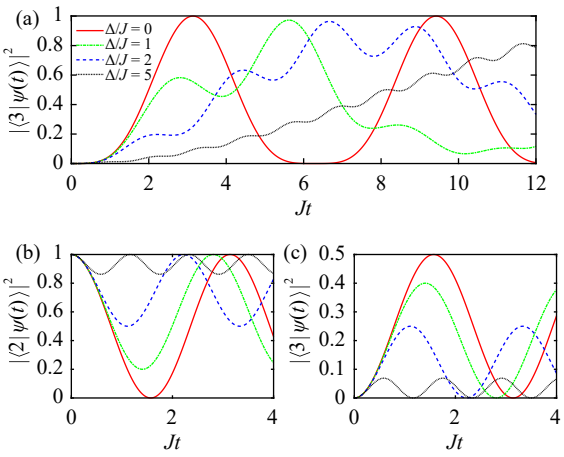

Fig. 2 The population dynamics on the intermediate site $|2\rangle$ and the target site $|3\rangle$ with different detunings Δs, where $J_{12} = J_{23} = J/\sqrt{2}$. The initial state is $|1\rangle$ in **(a)** and $|2\rangle$ in **(b)** and **(c)**. Solid red, dash-dotted green, dashed blue, and dotted black lines denote $\Delta/J = 0, 1, 2, 5$, respectively.

becomes slower with larger Δ. Although the dark eigenstate has zero amplitude on site 2, the initial state $|1\rangle$ contains both dark and bright components. The bright components have nonzero intermediate-site amplitudes, and their evolving relative phases can produce a finite population on site 2. In contrast, Figs. 2(b) and (c) start from the intermediate site, $|\psi(0)\rangle = |2\rangle = \sin\phi|b_+\rangle - \cos\phi|b_-\rangle$, which has no overlap with the dark state. These panels therefore illustrate bright-state dynamics and show how detuning inhibits the escape of an excitation initially occupying site 2. When $\Delta = 0$, the excitation on $|2\rangle$ can be completely transferred out during the evolution. As Δ increases, the minimum population on $|2\rangle$ rises and the maximum population on $|3\rangle$ decreases, indicating that more excitation is trapped on site 2 and therefore cannot reach site 3. To maximize the energy-transfer efficiency, Δ should be tuned to zero. Such tuning of the site energy can be implemented via the Stark effect [63–73], e.g., by applying a local electric field to the relevant site. The equal-coupling case in Fig. 2 is chosen for illustration and is not required for the existence of the dark state. For the isolated resonant bridge with the excitation initially localized on site 1, coupling asymmetry reduces the maximum population transferred to site 3 through the factor $\sin^2(2\theta)$. In the following section, we consider the unequal couplings of the PSI-derived bridge.

3 Efficiency in the natural PSI

For a natural photosynthesis system such as PSI which contains 96 sites, the efficiency is optimized during millions of years of evolution. To highlight the effect of our level-modulating proposal, we only investigate part

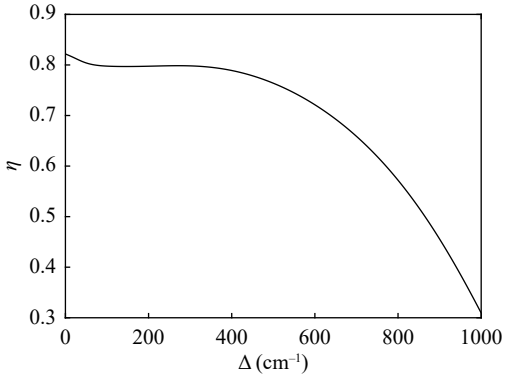

Fig. 3 The effect of the intermediate site detuning Δ on the energy transfer efficiency η of the bridge, with $J_{12} = 43.72\ \mathrm{cm}^{-1}$, $J_{23} = 12.82\ \mathrm{cm}^{-1}$, $J_{13} = -0.44\ \mathrm{cm}^{-1}$ from the cluster A4-A28-A40 in PSI, $\kappa^{-1} = 1$ ns, and $\Gamma'^{-1} = 10$ ps.

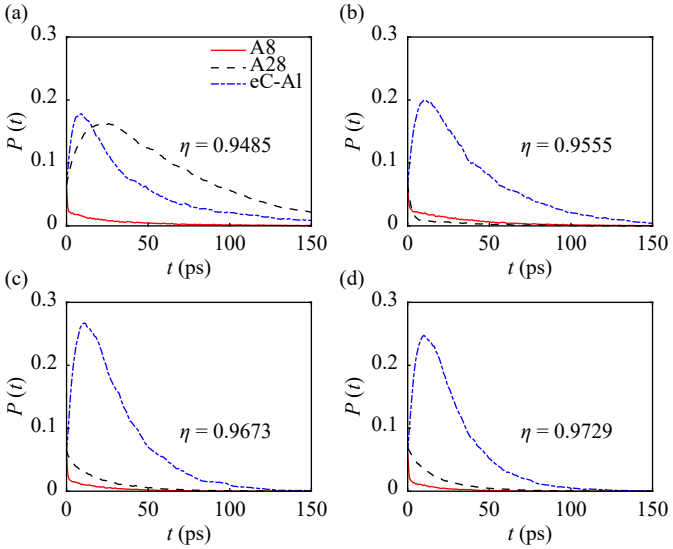

Fig. 4 The population dynamics of the OA, the RC and the bridge with $\kappa^{-1} = 1$ ns and $\Gamma^{-1} = 10$ ps. The level structure is **(a)** "extremely bad" with $\Delta = 1000\ \mathrm{cm}^{-1}$, **(b)** the same as the natural PSI, **(c)** modified to $E_1 = E_2 = E_3 = 14006\ \mathrm{cm}^{-1}$, **(d)** modified to $E_1 = E_2 = E_3 = 13940\ \mathrm{cm}^{-1}$, whose efficiency $\eta = 0.9729$ is the highest in the parameter regime.

of the total system, as shown in Fig. 1(b). The partial network contains six sites in the OA, i.e., A8, A10, A11, A18, A19 and A20, the RC with six sites, and the bridge, i.e., A4, A28 and A40, whose energies of the excited state are modified in our scheme while the couplings are the same as the natural PSI. The selected 15-site subsystem retains the three functional components required to examine the proposed mechanism: an outer antenna, a connecting bridge, and a reaction center with charge separation. This reduced network allows us to investigate the influence of bridge-energy tuning while retaining PSI-derived site parameters and couplings. It is intended to illustrate the bridge mechanism rather than reproduce all transport pathways of the complete 96-site complex. We first investigate the mechanism of the simplified three-site bridge model shown in Fig. 1(a), where A4, A28, and A40 correspond to sites 1, 2, and 3, respectively. The initial excitation is on site 1. The coupling constants are $J_{12} = 43.72\ \mathrm{cm}^{-1}$, $J_{23} = 12.82\ \mathrm{cm}^{-1}$, and $J_{13} = -0.44\ \mathrm{cm}^{-1} \ll J_{12}, J_{23}$ [47]. We tune $E_1 = E_3$ to satisfy the two-photon resonance condition for EIT. The spontaneous-emission rate $\kappa^{-1} = 1$ ns [74], and the effective charge-separation rate $\Gamma'^{-1} = 10$ ps [16]. As shown in Fig. 3, the efficiency decreases as the detuning Δ increases, because more energy becomes trapped on site 2, enhancing the effect of dissipation.

Next, we connect the OA and the RC through the bridge A4-A28-A40. We investigate the evolution of the system via the CMRT, where the population-transfer rates R_{ij}'s are derived from the Hamiltonian of the 15-site network [49, 57]. The spontaneous-emission rate is $\kappa^{-1} = 1$ ns [74]. We consider eC-A1 in the RC as the destination of the energy transfer, whose charge-separation rate is $\Gamma^{-1} = 10$ ps [16]. The efficiency η of the light-harvesting network is derived by integrating the population on the excited state of the RC site eC-A1, i.e., $\eta = \Gamma \int_0^\infty \langle \mathrm{eC-A1}|\rho(t)|\mathrm{eC-A1}\rangle \mathrm{d}t$. The initial state is the maximally mixed state of all 15 sites, i.e., $\rho(0) = I/15$. In Fig. 4, we present the population dynamics on A8 in the OA, the intermediate site A28 in the bridge, and the RC site eC-A1. In Fig. 4(a), we investigate the large-detuning case with two-photon resonance, i.e., $E_1 = E_3$ and $\Delta = 1000\ \mathrm{cm}^{-1} \gg J_{12}, J_{23}$. The efficiency is $\eta = 0.9485$. For comparison, we also present the dynamics of the system where the excitation energy of each site is the same as in the natural PSI, as shown in Fig. 4(b). The efficiency of the large-detuning case is lower than the natural PSI. This is because when the detuning Δ is large, the population on the intermediate site A28 cannot be effectively transported to other sites, which has been demonstrated in Fig. 2. Thus, in this condition, A28 becomes an obstacle of the energy-transfer process, thereby limiting the efficiency of the whole system.

Finally, we modify the three bridge-site energies to satisfy both single-photon and two-photon resonance, i.e., $E_1 = E_2 = E_3 = E$, where $E = 14006\ \mathrm{cm}^{-1}$ is the site energy of A4 in natural PSI. As shown in Fig. 4(c), when the excitation energies of the three bridge sites are on resonance, the populations on the OA sites and bridge sites decrease more rapidly than in the cases in Figs. 4(a) and (b), which indicates that the energy is transferred to the RC more quickly. Therefore, the spontaneous-emission decay of the OA and bridge sites is decreased if the level structure of the 3-site cluster is resonant, and the energy-transfer efficiency of the network increases. The results in Fig. 4 indicate that the energy-transfer efficiency of the whole system will increase if we modulate the level structure of the 3-site cluster to be resonant.

For an isolated three-site bridge, shifting all three site energies by the same amount does not change its internal population dynamics. In the full network, however, the

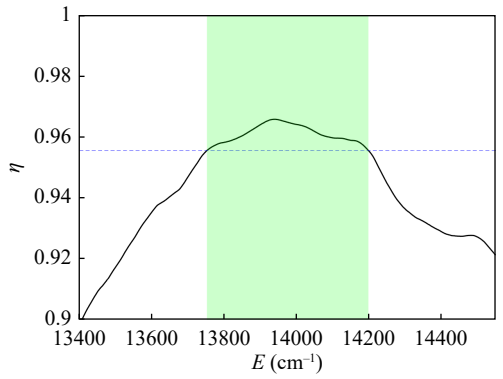

Fig. 5 The energy-transfer efficiency of the light-harvesting network where the energy levels of the bridge are modified to be $E_1 = E_2 = E_3 = E$. Dashed line represents the efficiency where the energy levels of the bridge are the same as the natural PSI. In the green area, i.e. $13752\,\mathrm{cm}^{-1} < E < 14199\,\mathrm{cm}^{-1}$, the bridge with modified energy levels works better than the natural PSI.

antenna and reaction-center energies remain fixed. Varying the common bridge energy E therefore changes the energetic alignment between the bridge and the surrounding sites, modifying the corresponding transfer rates. Thus, we also investigate the influence of E on the efficiency, as shown in Fig. 5. The numerical data are smoothed using a Savitzky–Golay filter [75] for visualization. Although internal resonance is maintained throughout Fig. 5, the efficiency depends on how effectively excitation enters and leaves the bridge. When $13752\,\mathrm{cm}^{-1} < E < 14199\,\mathrm{cm}^{-1}$, the bridge with modified energy levels works better than the natural PSI. The optimal range lies between the lowest excited-state energy of the RC, i.e., 13201 cm^{-1} and the highest excited-state energy of the OA i.e., 14513 cm^{-1}. The maximum efficiency, $\eta = 0.9729$, is achieved at $E = 13940\,\mathrm{cm}^{-1}$, as shown in Fig. 4(d).

4 Efficiency in the artificial light-harvesting system

Furthermore, we investigate the performance of the bridge in an artificial light-harvesting system. The OA contains 19 sites that form a regular octahedron with side length being $2\sqrt{2}$ nm. The RC contains 6 sites that also form a regular octahedron with a side length equal to $\sqrt{2}$ nm. The bridge contains 3 sites. The distance between nearest neighbors in the A19-B1-B2-B3-R1 chain is 1.5 nm. The dipole moment of each site is 5.2384 Debye [47]. The dipole-moment orientation of A1-A19 and B1 is along the x direction, while the orientation of R1–R6 and B3 is along the z direction. The dipole-moment orientation of B2 is along the bisector of the x and z axes. We assume the charge-separation process occurs on R6.

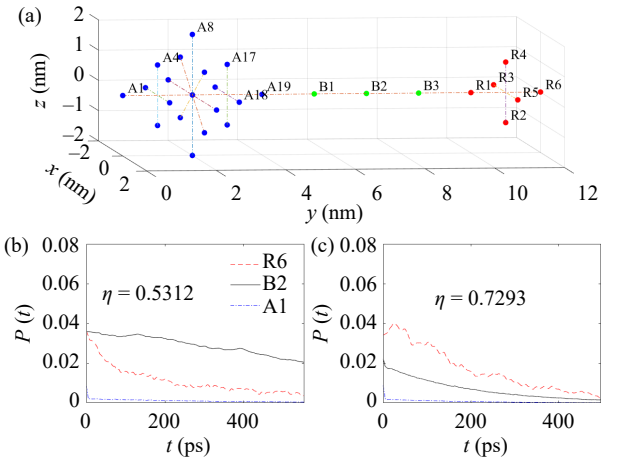

Fig. 6 **(a)** Diagram of the artificial light-harvesting system. The OA contains 19 sites, i.e., A1 to A19. The RC contains 6 sites i.e., R1 to R6. The bridge contains 3 sites i.e., B1 to B3. The dipole moment of each site is 5.2384 Debye. The dipole-moment orientation of A1-A19 and B1 is along the x direction, while the orientation of R1-R6 and B3 is along the z direction. The dipole-moment orientation of B2 is along the bisector of the x and z axes. **(b, c)** The population dynamics of the outer antenna and the bridge with $\kappa^{-1} = 1$ ns and $\Gamma^{-1} = 10$ ps. The level structure is (b) "extremely bad" with $\Delta = 1000\,\mathrm{cm}^{-1}$, (c) modified to $E_1 = E_2 = E_3 = 14100\,\mathrm{cm}^{-1}$.

We first insert a large-detuning bridge with site energies being respectively $E_1 = E_3 = 14100\,\mathrm{cm}^{-1}$ and $E_2 = 13100\,\mathrm{cm}^{-1}$. Here E_1, E_2 and E_3 are the site energies of B1, B2 and B3, respectively. The initial state is the maximally mixed state of all 28 sites, i.e., $\rho(0) = I/28$. The efficiency is 0.5312. The population on B2, i.e., the intermediate site of the bridge, cannot be efficiently transferred to the other sites, as shown in Fig. 6(b). Next, we modify the site energy E_2 to be resonant with E_1 and E_3. In this case, the populations on the OA and the bridge are transferred to the RC much faster than the large-detuning case, as shown in Fig. 6(c). Therefore, the efficiency is increased to 0.7293. The artificial structure is intended to test the bridge-tuning mechanism in a network distinct from the PSI-derived subsystem, rather than to provide a fully optimized light-harvesting architecture. Its geometry, coupling network, site-energy arrangement, and number of sites differ from those of the PSI example, so the absolute efficiencies are not directly comparable. Figure 6 demonstrates the applicability of bridge-energy tuning to an additional artificial architecture. Bringing the bridge into resonance alleviates the transport bottleneck.

5 Conclusion and remarks

In this paper, we investigate the energy-transfer process in both natural and artificial photosynthetic systems.

We focus on the bridge connecting the RC and the OA far away from the RC. We find that by modulating the level structure of the 3-site bridge to be resonant, the energy transfer becomes faster and more efficient with the assistance of the dark state, and the total energy-transfer efficiency will be enhanced. The bridge-assisted transfer mechanism can also be applied to artificial light-harvesting structures, providing useful guidance for the design of high-performance artificial systems.

Declarations The authors declare that they have no competing interests and there are no conflicts.

Acknowledgements We thank Prof. Y. C. Cheng for introducing the interesting issue of PSI to us. This work was supported by the Quantum Science and Technology-National Science and Technology Major Project (No. 2023ZD0300200), the National Natural Science Foundation of China under Grant No. 62461160263, and the Guangdong Provincial Quantum Science Strategic Initiative under Grant No. GDZX2505004.

Appendix A: The derivation of the master equation

In this part, we demonstrate the detailed derivation of the master equation using the CMRT. The Hamiltonian of the system is

$$H_S = \sum_n E_n|n\rangle\langle n| + \sum_{m\neq n} J_{mn}|m\rangle\langle n| = \sum_k \varepsilon'_k|\varepsilon_k\rangle\langle\varepsilon_k|, \tag{A1}$$

where $|n\rangle$ represents the excitation on the site n with energy E_n while the other sites are in the ground state, J_{mn} is the coupling between $|n\rangle$ and $|m\rangle$. The eigen state $|\varepsilon_k\rangle$ with exciton energy ε'_k is a superposition of site bases as $|\varepsilon_k\rangle = \sum_n C_{nk}|n\rangle$.

The environment could be modeled as a collection of harmonic oscillators described by the Hamiltonian

$$H_E = \sum_{n,q}\left(\frac{p_{nq}^2}{2m_q} + \frac{1}{2}m_q\omega_q^2 x_{nq}^2\right) = \sum_{n,q}\omega_q a_{nq}^\dagger a_{nq}, \tag{A2}$$

where $a_{nq}^\dagger$ is the creation operator of qth harmonic oscillator of site n with frequency ω_q, and $x_{nq} = (a_{nq}^\dagger + a_{nq})/\sqrt{2m_q\omega_q}$, $p_{nq} = \mathrm{i}\sqrt{m_q\omega_q/2}(a_{nq}^\dagger - a_{nq})$ are the coordinate operator and the momentum operator of the site n. The interaction between the system and the environment is described by the Hamiltonian

$$H_{SE} = \sum_{n,q} g_{nq}\omega_q(a_{nq}^\dagger + a_{nq})|n\rangle\langle n| = \sum_{k,k'} u_{kk'}|\varepsilon_k\rangle\langle\varepsilon_{k'}|, \tag{A3}$$

where g_{nq} is a dimensionless coupling constant, $u_{kk'} = \sum_{n,q} A_{kk'}(n)g_{nq}\omega_q(a_{nq}^\dagger + a_{nq})$, and $A_{kk'}(n) = C_{nk}^* C_{nk'}$. The total Hamiltonian is the sum of these three parts, i.e., $H = H_S + H_E + H_{SE}$.

According to the CMRT [49, 57], the total Hamiltonian could be divided into the zeroth-order Hamiltonian including the diagonal system-bath interaction in the exciton basis, i.e., $H_0 = \sum_k(\varepsilon'_k + u_{kk})|\varepsilon_k\rangle\langle\varepsilon_k| + H_E$, and a perturbation Hamiltonian, i.e., the off-diagonal system-bath interaction as $V = \sum_{k\neq k'} u_{kk'}|\varepsilon_k\rangle\langle\varepsilon_{k'}|$. Using the completeness relation, we rewrite H_0 as

$$H_0 = \sum_k\left[\varepsilon_k + H_E(A_{kk}(n)x_{nq}^{(0)})\right]|\varepsilon_k\rangle\langle\varepsilon_k|, \tag{A4}$$

where

$$\varepsilon_k = \varepsilon'_k - \Lambda_k, \tag{A5}$$

$$\begin{aligned}\Lambda_k &= \frac{1}{2}\sum_{n,q} A_{kk}^2(n)m_q\omega_q^2(x_{nq}^{(0)})^2 \\ &= \sum_n A_{kk}^2(n)\lambda_n,\end{aligned} \tag{A6}$$

$$H_E(A_{kk}(n)x_{nq}^{(0)}) = \sum_{n,q}\left[\frac{p_{nq}^2}{2m_q} + \frac{1}{2}m_q\omega_q^2(x_{nq} + A_{kk}x_{nq}^{(0)})^2\right]. \tag{A7}$$

We define that $\chi(t)$ is the density operator for the total system including the system and the environment, and $\rho(t) = \mathrm{tr}_E[\chi(t)]$ is the reduced density matrix of the system. The von Neumann-Liouville equation for $\chi(t)$ reads

$$\dot{\chi}(t) = -\mathrm{i}[H, \chi]. \tag{A8}$$

Transforming Eq. (A8) into the interaction picture with respect to H_0, and considering the weak-coupling approximation and the Markovian approximation, we have the second-order equation of motion for the reduced density matrix $\rho(t)$ as

$$\dot{\rho} = -\mathrm{i}[H_0, \rho] - \int_0^t \mathrm{tr}_E[V, [V(-\tau), \rho(t)\rho_E]]\mathrm{d}\tau, \tag{A9}$$

where $\tau = t - t'$ and $V(-\tau) = \exp(-\mathrm{i}H_0\tau)V\exp(\mathrm{i}H_0\tau)$.

The explicit form of the equation of motion contains two parts, i.e., the diagonal elements and the off-diagonal elements. The equations of motion for diagonal elements are

$$\begin{aligned}\dot{\rho}_{k'k'} = &-\mathrm{i}\langle\varepsilon_{k'}|[H_0, \rho]|\varepsilon_{k'}\rangle - \sum_{k(\neq k')} R_{kk'}^{dis}(t)\rho_{k'k'} \\ &+ \sum_{k(\neq k')} R_{k'k}^{dis}(t)\rho_{kk},\end{aligned} \tag{A10}$$

with the dissipation rate

$$R^{dis}_{kk'}(t) = 2\mathrm{Re}\int_0^t \mathrm{d}\tau \mathrm{e}^{-\mathrm{i}(\varepsilon_k-\varepsilon_{k'})\tau}\mathrm{e}^{-[g_{kkkk}(\tau)+g_{k'k'k'k'}(\tau)-2g_{kkk'k'}(\tau)]}\mathrm{e}^{-\mathrm{i}(\Lambda_k+\Lambda_{k'}-2\lambda_{kkk'k'})\tau} \times \{\ddot{g}_{k'kkk'}(\tau) - [\dot{g}_{k'kkk}(\tau) - \dot{g}_{k'kk'k'}(\tau) - 2\mathrm{i}\lambda_{k'kk'k'}][\dot{g}_{kk'kk}(\tau) - \dot{g}_{kk'k'k'}(\tau) - 2\mathrm{i}\lambda_{kk'k'k'}]\}, \tag{A11}$$

where

$$g_{k_1k_2k_3k_4}(t) = \sum_n A_{k_1k_2}(n)A_{k_3k_4}(n)g_n(t), \tag{A12}$$

$$\lambda_{k_1k_2k_3k_4} = \sum_n A_{k_1k_2}(n)A_{k_3k_4}(n)\lambda_n, \tag{A13}$$

$$g_n(t) = \int_0^\infty \mathrm{d}\omega \frac{J_n(\omega)}{\omega^2}\left[(1-\cos\omega t)\coth\left(\frac{\omega}{2k_BT}\right) + \mathrm{i}(\sin\omega t - \omega t)\right]. \tag{A14}$$

For the off-diagonal elements, we can calculate directly from the von Neumann-Liouville equation Eq. (A8) and obtain

$$\dot{\rho}_{kk'} = -\mathrm{i}(\varepsilon_k - \varepsilon_{k'})\rho_{kk'} - R^{pd}_{kk'}(t)\rho_{kk'}, \tag{A15}$$

where the pure-dephasing rate is

$$R^{pd}_{kk'}(t) = \sum_n [A_{kk}(n) - A_{k'k'}(n)]^2\mathrm{Re}[\dot{g}_n(t)]. \tag{A16}$$

Taking into account both dissipation and pure dephasing, we obtain the complete master equation

$$\begin{aligned}\partial_t\rho = &-\mathrm{i}[H_S(t),\rho] \\ &-\frac{1}{2}\sum_{k\neq k'} R^{dis}_{kk'}(t)\left[\left\{\mathcal{A}^\dagger_{kk'}\mathcal{A}_{kk'},\rho\right\} - 2\mathcal{A}_{kk'}\rho\mathcal{A}^\dagger_{kk'}\right] \\ &-\sum_{k\neq k'} R^{pd}_{kk'}(t)\rho_{kk'}\mathcal{A}_{kk'},\end{aligned} \tag{A17}$$

where $\left\{\mathcal{A}^\dagger_{kk'}\mathcal{A}_{kk'},\rho\right\}$ denotes the anticommutator and $\mathcal{A}_{kk'} = |\varepsilon_k\rangle\langle\varepsilon_{k'}|$ are the jump operators.

For further simplification, we could rewrite the pure-dephasing term in the Lindblad form. Noticing that $\mathcal{A}^\dagger_{kk}\mathcal{A}_{kk} = \mathcal{A}_{kk} = \mathcal{A}^\dagger_{kk} = |\varepsilon_k\rangle\langle\varepsilon_k|$, we have

$$\begin{aligned}&-\sum_k \frac{\Gamma_k}{2}\left[\{\mathcal{A}^\dagger_{kk}\mathcal{A}_{kk},\rho\} - 2\mathcal{A}_{kk}\rho\mathcal{A}^\dagger_{kk}\right] \\ &\quad = -\sum_k\sum_{k'(\neq k)}\frac{\Gamma_k+\Gamma_{k'}}{2}\mathcal{A}_{kk'}\rho_{kk'}.\end{aligned} \tag{A18}$$

Therefore, if we could rewrite the pure-dephasing rate as $R^{pd}_{kk'}(t) = (\Gamma_k+\Gamma_{k'})/2$, the pure-dephasing term can be written in the Lindblad form

$$\begin{aligned}&-\sum_{k\neq k'} R^{pd}_{kk'}(t)\rho_{kk'}\mathcal{A}_{kk'} \\ &\quad = -\sum_k \frac{\Gamma_k}{2}\left[\{\mathcal{A}^\dagger_{kk}\mathcal{A}_{kk},\rho\} - 2\mathcal{A}_{kk}\rho\mathcal{A}^\dagger_{kk}\right].\end{aligned} \tag{A19}$$

Assuming that the total number of the sites is N, there are $N(N-1)/2$ independent pure-dephasing rates $R^{pd}_{kk'}$ but only N Lindblad form pure-dephasing rates Γ_k. Thus we need some additional constraints to determine $\Gamma_{k'}$. Here we adopt the least-squares fitting method in Ref. [57] to determine $\boldsymbol{\Gamma} = (\Gamma_1,\Gamma_2,\cdots,\Gamma_N)^{\mathrm{T}}$, which gives

$$\boldsymbol{\Gamma} = \boldsymbol{Q}^{-1}\boldsymbol{P}, \tag{A20}$$

$$P_a = \sum_{k=a+1}^{N} R^{pd}_{ak} + \sum_{k=1}^{N-1} R^{pd}_{ka}, \tag{A21}$$

$$Q_{jk} = \begin{cases} N-j/2, & \text{for } k=j, \\ 1, & \text{for } j<k<N, \\ 1/2, & \text{otherwise.}\end{cases} \tag{A22}$$

Finally, the original master equation Eq. (A17) can be rewritten in the Lindblad form as

$$\begin{aligned}\partial_t\rho = &-\mathrm{i}[H_S(t),\rho] \\ &-\frac{1}{2}\sum_{k,k'} R_{kk'}(t)\left[\left\{\mathcal{A}^\dagger_{kk'}\mathcal{A}_{kk'},\rho\right\} - 2\mathcal{A}_{kk'}\rho\mathcal{A}^\dagger_{kk'}\right],\end{aligned} \tag{A23}$$

where the matrix elements of the population transfer and dephasing rates $R_{kk'}$ are defined respectively as

$$R_{kk'} \equiv \begin{cases} R^{dis}_{kk'}(t), & \text{for } k\neq k', \\ \Gamma_k, & \text{for } k=k'.\end{cases} \tag{A24}$$

References

1. B. Rybtchinski, L. E. Sinks, and M. R. Wasielewski, Combining light-harvesting and charge separation in a self-assembled artificial photosynthetic system based on perylenediimide chromophores, *J. Am. Chem. Soc.* 126(39), 12268 (2004)
2. S. Fukuzumi, Development of bioinspired artificial photosynthetic systems, *Phys. Chem. Chem. Phys.* 10(17), 2283 (2008)
3. S. Y. Reece, J. A. Hamel, K. Sung, T. D. Jarvi, A. J. Esswein, J. J. H. Pijpers, and D. G. Nocera, Wireless solar water splitting using silicon-based semiconductors

and earth-abundant catalysts, *Science* 334(6056), 645 (2011)
4. L. Alibabaei, B. D. Sherman, M. R. Norris, M. K. Brennaman, and T. J. Meyer, Visible photoelectrochemical water splitting into H_2 and O_2 in a dye-sensitized photoelectrosynthesis cell, *Proc. Natl. Acad. Sci. USA* 112(19), 5899 (2015)
5. B. Turan, J. P. Becker, F. Urbain, F. Finger, U. Rau, and S. Haas, Upscaling of integrated photoelectrochemical water-splitting devices to large areas, *Nat. Commun.* 7(1), 12681 (2016)
6. F. A. Chowdhury, M. L. Trudeau, H. Guo, and Z. T. Mi, A photochemical diode artificial photosynthesis system for unassisted high efficiency overall pure water splitting, *Nat. Commun.* 9(1), 1707 (2018)
7. K. P. Sokol, W. E. Robinson, J. Warnan, N. Kornienko, M. M. Nowaczyk, A. Ruff, J. Z. Zhang, and E. Reisner, Bias-free photoelectrochemical water splitting with photosystem II on a dye-sensitized photoanode wired to hydrogenase, *Nat. Energy* 3(11), 944 (2018)
8. L. Q. Zhou, C. Ling, H. Zhou, X. Wang, J. Liao, et al, A high-performance oxygen evolution catalyst in neutral-pH for sunlight-driven CO_2 reduction, *Nat. Commun.* 10(1), 4081 (2019)
9. D. K. Dogutan and D. G. Nocera, Artificial photosynthesis at efficiencies greatly exceeding that of natural photosynthesis, *Acc. Chem. Res.* 52(11), 3143 (2019)
10. Z. F. Wang, Y. Hu, S. P. Zhang, and Y. Sun, Artificial photosynthesis systems for solar energy conversion and storage: Platforms and their realities, *Chem. Soc. Rev.* 51(15), 6704 (2022)
11. Y. Wang, J. X. Wei, H. L. Tang, L. H. Shao, L. Z. Dong, X. Y. Chu, Y. X. Jiang, G. L. Zhang, F. M. Zhang, and Y. Q. Lan, Artificial photosynthetic system for diluted CO_2 reduction in gas-solid phase, *Nat. Commun.* 15(1), 8818 (2024)
12. S. Mori, R. Hashimoto, T. Hisatomi, K. Domen, and S. Saito, Artificial photosynthesis directed toward organic synthesis, *Nat. Commun.* 16(1), 1797 (2025)
13. Y. Mazor, A. Borovikova, I. Caspy, and N. Nelson, Structure of the plant photosystem I supercomplex at 2.6 Å resolution, *Nat. Plants* 3(3), 17014 (2017)
14. X. P. Wei, X. D. Su, P. Cao, X. Y. Liu, W. R. Chang, M. Li, X. Z. Zhang, and Z. F. Liu, Structure of spinach photosystem II–LHCII supercomplex at 3.2 Å resolution, *Nature* 534(7605), 69 (2016)
15. R. Croce and H. van Amerongen, Light harvesting in oxygenic photosynthesis: Structural biology meets spectroscopy, *Science* 369(6506), eaay2058 (2020)
16. N. Nelson and W. Junge, Structure and energy transfer in photosystems of oxygenic photosynthesis, *Annu. Rev. Biochem.* 84, 659 (2015)
17. X. C. Qin, M. Suga, T. Y. Kuang, and J. R. Shen, Structural basis for energy transfer pathways in the plant PSI-LHCI supercomplex, *Science* 348(6238), 989 (2015)
18. X. W. Pan, J. Ma, X. D. Su, P. Cao, W. R. Chang, Z. F. Liu, X. Z. Zhang, and M. Li, Structure of the maize photosystem I supercomplex with light-harvesting complexes I and II, *Science* 360(6393), 1109 (2018)
19. M. Iwai, P. Grob, A. T. Iavarone, E. Nogales, and K. K. Niyogi, A unique supramolecular organization of photosystem I in the moss *Physcomitrella patens*, *Nat. Plants* 4(11), 904 (2018)
20. X. C. Qin, X. Pi, W. D. Wang, G. Y. Han, L. X. Zhu, M. M. Liu, L. P. Cheng, J. R. Shen, T. Y. Kuang, and S. F. Sui, Structure of a green algal photosystem I in complex with a large number of light-harvesting complex I subunits, *Nat. Plants* 5(3), 263 (2019)
21. A. Stirbet, D. Lazár, Y. Guo, and G. Govindjee, Photosynthesis: basics, history and modelling, *Ann. Bot.* 126(4), 511 (2020)
22. I. Caspy, A. Borovikova-Sheinker, D. Klaiman, Y. Shkolnisky, and N. Nelson, The structure of a triple complex of plant photosystem I with ferredoxin and plastocyanin, *Nat. Plants* 6(10), 1300 (2020)
23. R. Nagao, K. Kato, K. Ifuku, T. Suzuki, M. Kumazawa, et al, Structural basis for assembly and function of a diatom photosystem I-light-harvesting supercomplex, *Nat. Commun.* 11(1), 2481 (2020)
24. D. Harris, H. Toporik, G. S. Schlau-Cohen, and Y. Mazor, Energetic robustness to large scale structural fluctuations in a photosynthetic supercomplex, *Nat. Commun.* 14(1), 4650 (2023)
25. A. Wilde, H. Härtel, T. Hübschmann, P. Hoffmann, S. V. Shestakov, and T. Börner, Inactivation of a *Synechocystis* sp strain PCC 6803 gene with homology to conserved chloroplast open reading frame 184 increases the photosystem II-to-photosystem I ratio, *Plant Cell* 7(5), 649 (1995)
26. J. Stöckel, S. Bennewitz, P. Hein, and R. Oelmüller, The evolutionarily conserved tetratrico peptide repeat protein pale yellow green7 is required for photosystem I accumulation in arabidopsis and copurifies with the complex, *Plant Physiol.* 141(3), 870 (2006)
27. C. A. Albus, S. Ruf, M. A. Schöttler, W. Lein, J. Kehr, and R. Bock, Y3IP1, a nucleus-encoded thylakoid protein, cooperates with the plastid-encoded Ycf3 protein in photosystem I assembly of tobacco and *Arabidopsis*, *Plant Cell* 22(8), 2838 (2010)
28. J. Liu, H. X. Yang, Q. T. Lu, X. G. Wen, F. Chen, L. W. Peng, L. X. Zhang, and C. M. Lu, PSBP-DOMAIN PROTEIN1, a nuclear-encoded thylakoid lumenal protein, is essential for photosystem I assembly in *Arabidopsis*, *Plant Cell* 24(12), 4992 (2012)
29. J. Shen, R. Williams-Carrier, and A. Barkan, PSA3, a protein on the stromal face of the thylakoid membrane, promotes photosystem I accumulation in cooperation with the assembly factor PYG7, *Plant Physiol.* 174(3), 1850 (2017)
30. S. Nellaepalli, S. I. Ozawa, H. Kuroda, and Y. Takahashi, The photosystem I assembly apparatus consisting of Ycf3–Y3IP1 and Ycf4 modules, *Nat. Commun.* 9(1), 2439 (2018)
31. X. D. Su, J. Ma, X. W. Pan, X. L. Zhao, W. R. Chang, Z. F. Liu, X. Z. Zhang, and M. Li, Antenna arrangement and energy transfer pathways of a green algal photosystem-I–LHCI supercomplex, *Nat. Plants* 5(3), 273 (2019)
32. M. Suga, S. I. Ozawa, K. Yoshida-Motomura, F. Akita, N. Miyazaki, and Y. Takahashi, Structure of the green algal photosystem I supercomplex with a decameric light-harvesting complex I, *Nat. Plants* 5(6), 626 (2019)

33. G. Garab, M. Magyar, G. Sipka, and P. H. Lambrev, New foundations for the physical mechanism of variable chlorophyll *a* fluorescence: Quantum efficiency versus the light-adapted state of photosystem II, *J. Exp. Bot.* 74(18), 5458 (2023)
34. X. You, X. Zhang, J. Cheng, Y. N. Xiao, J. F. Ma, S. Sun, X. Z. Zhang, H. W. Wang, and S. F. Sui, In situ structure of the red algal phycobilisome–PSII–PSI–LHC megacomplex, *Nature* 616(7955), 199 (2023)
35. Y. Feng, Z. H. Li, X. Y. Li, L. L. Shen, X. Y. Liu, et al, Structure of a diatom photosystem II supercomplex containing a member of Lhcx family and dimeric FCPII, *Sci. Adv.* 9(43), eadi8446 (2023)
36. A. H. Zhang, L. Tian, T. Zhu, M. Y. Li, M. W. Sun, Y. Fang, Y. Zhang, and C. M. Lu, Uncovering the photosystem I assembly pathway in land plants, *Nat. Plants* 10(4), 645 (2024)
37. M. Fleischhauer, A. Imamoglu, and J. P. Marangos, Electromagnetically induced transparency: optics in coherent media, *Rev. Mod. Phys.* 77(2), 633 (2005)
38. Q. C. Liu, T. F. Li, X. Q. Luo, H. Zhao, W. Xiong, et al, Method for identifying electromagnetically induced transparency in a tunable circuit quantum electrodynamics system, *Phys. Rev. A* 93(5), 053838 (2016)
39. X. Gu, S. N. Huai, F. Nori, and Y. X. Liu, Polariton states in circuit QED for electromagnetically induced transparency, *Phys. Rev. A* 93(6), 063827 (2016)
40. X. Wang, A. Miranowicz, H. R. Li, F. L. Li, and F. Nori, Two-color electromagnetically induced transparency via modulated coupling between a mechanical resonator and a qubit, *Phys. Rev. A* 98(2), 023821 (2018)
41. Y. Y. Wang, J. Qiu, Y. Q. Chu, M. Zhang, J. M. Cai, Q. Ai, and F. G. Deng, Dark state polarizing a nuclear spin in the vicinity of a nitrogen–vacancy center, *Phys. Rev. A* 97(4), 042313 (2018)
42. C. Q. Wang, X. F. Jiang, G. M. Zhao, M. Z. Zhang, C. W. Hsu, B. Peng, A. D. Stone, L. Jiang, and L. Yang, Electromagnetically induced transparency at a chiral exceptional point, *Nat. Phys.* 16(3), 334 (2020)
43. G. Andersson, M. K. Ekström, and P. Delsing, Electromagnetically induced acoustic transparency with a superconducting circuit, *Phys. Rev. Lett.* 124(24), 240402 (2020)
44. K. McDonnell, L. F. Keary, and J. D. Pritchard, Demonstration of a quantum gate using electromagnetically induced transparency, *Phys. Rev. Lett.* 129(20), 200501 (2022)
45. B. Kim, K. T. Chen, K. Y. Chen, Y. S. Chiu, C. Y. Hsu, Y. H. Chen, and I. A. Yu, Experimental demonstration of stationary dark-state polaritons dressed by dipole-dipole interaction, *Phys. Rev. Lett.* 131(13), 133001 (2023)
46. H. Dong, D. Z. Xu, J. F. Huang, and C. P. Sun, Coherent excitation transfer *via* the dark-state channel in a bionic system, *Light Sci. Appl.* 1(3), e2 (2012)
47. A. Damjanović, H. M. Vaswani, P. Fromme, and G. R. Fleming, Chlorophyll excitations in photosystem I of *Synechococcus elongatus*, *J. Phys. Chem. B* 106(39), 10251 (2002)
48. M. Yang and G. R. Fleming, Influence of phonons on exciton transfer dynamics: comparison of the Redfield, Förster, and modified Redfield equations, *Chem. Phys.* 275(1-3), 355 (2002)
49. Y. H. Hwang-Fu, W. Chen, and Y. C. Cheng, A coherent modified Redfield theory for excitation energy transfer in molecular aggregates, *Chem. Phys.* 447, 46 (2015)
50. Y. Chang and Y. C. Cheng, On the accuracy of coherent modified Redfield theory in simulating excitation energy transfer dynamics, *J. Chem. Phys.* 142(3), 034109 (2015)
51. I. De Vega and D. Alonso, Dynamics of non-Markovian open quantum systems, *Rev. Mod. Phys.* 89(1), 015001 (2017)
52. S. J. Jang and B. Mennucci, Delocalized excitons in natural light-harvesting complexes, *Rev. Mod. Phys.* 90(3), 035003 (2018)
53. M. J. Tao, N. N. Zhang, P. Y. Wen, F. G. Deng, Q. Ai, and G. L. Long, Coherent and incoherent theories for photosynthetic energy transfer, *Sci. Bull.* 65(4), 318 (2020)
54. M. B. Plenio and P. L. Knight, The quantum-jump approach to dissipative dynamics in quantum optics, *Rev. Mod. Phys.* 70(1), 101 (1998)
55. J. Piilo, S. Maniscalco, K. Härkönen, and K. A. Suominen, Non-Markovian quantum jumps, *Phys. Rev. Lett.* 100(18), 180402 (2008)
56. J. Piilo, K. Härkönen, S. Maniscalco, and K. A. Suominen, Open system dynamics with non-Markovian quantum jumps, *Phys. Rev. A* 79(6), 062112 (2009)
57. Q. Ai, Y. J. Fan, B. Y. Jin, and Y. C. Cheng, An efficient quantum jump method for coherent energy transfer dynamics in photosynthetic systems under the influence of laser fields, *New J. Phys.* 16(5), 053033 (2014)
58. H. P. Breuer and J. Piilo, Stochastic jump processes for non-Markovian quantum dynamics, *Europhys. Lett.* 85(5), 50004 (2009)
59. P. Rebentrost, R. Chakraborty, and A. Aspuru-Guzik, Non-Markovian quantum jumps in excitonic energy transfer, *J. Chem. Phys.* 131(18), 184102 (2009)
60. T. Becker, C. Netzer, and A. Eckardt, Quantum trajectories for time-local non-Lindblad master equations, *Phys. Rev. Lett.* 131(16), 160401 (2023)
61. R. Li, Y. Li, K. Y. Zhang, and Q. Ai, Quantum jump approach for photosynthetic energy transfer with chemical reaction and fluorescence loss, *Innovation Energy* 2(4), 100114 (2025)
62. J. L. Wu, R. J. Silbey, and J. S. Cao, Generic mechanism of optimal energy transfer efficiency: A scaling theory of the mean first-passage time in exciton systems, *Phys. Rev. Lett.* 110(20), 200402 (2013)
63. M. Saffman, T. G. Walker, and K. Mølmer, Quantum information with Rydberg atoms, *Rev. Mod. Phys.* 82(3), 2313 (2010)
64. J. A. Quirk, A. Jacobsen, A. Damitz, C. E. Tanner, and D. S. Elliott, Measurement of the static Stark shift of the $7s\ ^2S_{1/2}$ level in atomic cesium, *Phys. Rev. Lett.* 132(23), 233201 (2024)
65. S. A. Empedocles and M. G. Bawendi, Quantum-confined Stark effect in single CdSe nanocrystallite quantum dots, *Science* 278(5346), 2114 (1997)
66. T. LaMountain, J. Nelson, E. J. Lenferink, S. H. Amsterdam, A. A. Murthy, H. F. Zeng, T. J. Marks, V.

P. Dravid, M. C. Hersam, and N. P. Stern, Valley-selective optical Stark effect of exciton–polaritons in a monolayer semiconductor, *Nat. Commun.* 12(1), 4530 (2021)

67. S. Germanis, C. Katsidis, S. Tsintzos, A. Stavrinidis, G. Konstantinidis, et al., Enhanced Stark tuning of single InAs (211)B quantum dots due to nonlinear piezoelectric effect in zincblende nanostructures, *Phys. Rev. Appl.* 6(1), 014004 (2016)
68. S. Aghaeimeibodi, C. M. Lee, M. A. Buyukkaya, C. J. K. Richardson, and E. Waks, Large Stark tuning of InAs/InP quantum dots, *Appl. Phys. Lett.* 114(7), 071105 (2019)
69. J. Klein, J. Wierzbowski, A. Regler, J. Becker, F. Heimbach, K. Müller, M. Kaniber, and J. J. Finley, Stark effect spectroscopy of mono- and few-layer MoS_2, *Nano Lett.* 16(3), 1554 (2016)
70. C. Chakraborty, K. M. Goodfellow, S. Dhara, A. Yoshimura, V. Meunier, and A. N. Vamivakas, Quantum-confined Stark effect of individual defects in a van der Waals heterostructure, *Nano Lett.* 17(4), 2253 (2017)
71. J. G. Roch, N. Leisgang, G. Froehlicher, P. Makk, K. Watanabe, T. Taniguchi, C. Schönenberger, and R. J. Warburton, Quantum-confined Stark effect in a MoS_2 monolayer van der Waals heterostructure, *Nano Lett.* 18(2), 1070 (2018)
72. G. Noh, D. Choi, J. H. Kim, D. G. Im, Y. H. Kim, H. Seo, and J. Lee, Stark tuning of single-photon emitters in hexagonal boron nitride, *Nano Lett.* 18(8), 4710 (2018)
73. L. C. Bassett, F. J. Heremans, C. G. Yale, B. B. Buckley, and D. D. Awschalom, Electrical tuning of single nitrogen-vacancy center optical transitions enhanced by photoinduced fields, *Phys. Rev. Lett.* 107(26), 266403 (2011)
74. A. M. Gilmore, V. P. Shinkarev, T. L. Hazlett, and Govindjee, Quantitative analysis of the effects of intrathylakoid pH and xanthophyll cycle pigments on chlorophyll a fluorescence lifetime distributions and intensity in thylakoids, *Biochemistry* 37(39), 13582 (1998)
75. A. Savitzky and M. J. E. Golay, Smoothing and differentiation of data by simplified least squares procedures, *Anal. Chem.* 36(8), 1627 (1964)